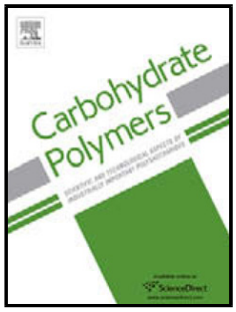

Title: Structural characterization and in vitro antitumor activity of A polysaccharide from *Artemisia annua* L. (Huang Huahao)

Authors: Liang Yan, Chuan Xiong, Pan Xu, Jing Zhu, Zhirong Yang, Hong Ren, Qiang Luo

PII: S0144-8617(19)30223-1
DOI: https://doi.org/10.1016/j.carbpol.2019.02.081
Reference: CARP 14654

To appear in:

Received date: 18 October 2018
Revised date: 29 January 2019
Accepted date: 24 February 2019

Please cite this article as: Yan L, Xiong C, Xu P, Zhu J, Yang Z, Ren H, Luo Q, Structural characterization and in vitro antitumor activity of A polysaccharide from *Artemisia annua* L. (Huang Huahao), *Carbohydrate Polymers* (2019), https://doi.org/10.1016/j.carbpol.2019.02.081

Structural characterization and in vitro antitumor activity of A polysaccharide from Artemisia annua L. (Huang Huahao)

LIANG YAN [a b], CHUAN XIONG [c], PAN XU [a], JING ZHU [b], ZHIRONG YANG [d], HONG REN [a], QIANG LUO [a,*]

[a] *Institute for Viral Hepatitis, Key Laboratory of Molecular Biology for Infectious Diseases, Chinese Ministry of Education, Department of Infectious Diseases, Second Affiliated Hospital of Chongqing Medical University, Chongqing 400010, China*

[b] *Pediatric Research Institute, Children's Hospital of Chongqing Medical University, Ministry of Education Key Laboratory of Child Development and Disorders, Chongqing 400014, China; China International Science and Technology Cooperation Base of Child Development and Critical Disorders, Chongqing 400014, China.*

[c] *Biotechnology and Nuclear Technology Research Institute, Sichuan Academy of Agricultural Sciences, Chengdu 610061, China*

[d] *Sichuan Province Key Laboratory of Nature Resources Microbiology and Technique, College of Life Sciences, Sichuan University, Chengdu, 610064, China*

[*] *Corresponding Author: QIANG LUO*

Email: qiangluo@email.com

Highlights

- **A polysaccharide was isolated and characterized from Artemisia annua L. (Huang Huahao)**
- **This polysaccharide induced apoptosis of HepG2 cell**
- **This polysaccharide-induced apoptosis is done via mitochondrial signaling pathway**

Abstract

One water-soluble polysaccharide (AAP), with a molecular weight of 6.3 × 104Da, was isolated from *Artemisia annua* L. Structrual analysis indicated that AAP was found to be a 1, 3-α-linked and 1, 3, 6-α-linked Glcp backbone, with a branch of 1, 6-α-linked Glcp and terminal 1-linked-L-Rhap along the main chain in a ratio of 1: 1: 1: 1. MTT assay showed that AAP reduced the cell viability of HepG2 cells in a concentration-dependent manner. DAPI staining and Flow cytometric analysis revealed that AAP suppressed cells proliferation, not most at least via inducing p65-dependent mitochondrial signaling pathway, as evidenced by more activation of caspase-3 and -9, down-regulation of Bcl-2 protein, up-regulation of Bax protein and release of cytochrome c from mitochondria into cytosol, as well as suppression of the nuclear factor-κB (NF-κB) p65. These data confirmed AAP inhibits HepG2 cell growth via inducing caspase-dependent mitochondrial apoptosis and inhibition of NF-κB p65.

Keywords: *Artemisia annua* L.; Huang Huahao; Polysaccharide; Antitumor activity;

Apoptosis; Nuclear factor-κB (NF-κB) p65

1. Introduction

Cancer is a leading dominant cause of human death globally. Chemotherapy is one of the most commonly applied and effective protocols for cancer treatment (Yang, Xiao, & Sun, 2013). However, the search for selective anticancer chemotherapeutic agents has not been fruitful to date, mainly due to their non-specific cytotoxicity and adverse effects, such as multidrug resistance of tumor cells, and especially, toxicity to normal cells (Bagchi et al., 2000; Krishna & Mayer, 2000). Recently, research interest has focused on polysaccharides from various plants and herbs with anitumor properties, which have been used in the prevention or treatment of cancer in many countries (Li et al., 2015; Liu, Sheng, Zhang, & Sun, 2016). Most polysaccharides derived from various natural sources are believed that have superior anti-tumor activities and do not causes significant side effects compared with synthetic compounds (Chen et al., 2013; Sun et al., 2014; Wang et al., 2013). Therefore, discovery and evaluation of polysaccharides with antitumor properties and low

toxicity have emerged as one of the most attractive strategies against cancer.

Hua Huahao (*Artemisia annua* L.) is an annual plant native of the Asian continent and has been traditionally used throughout the ages for the treatment of malaria (Räth et al., 2004). In addition, *A. annua* are also reported to have significant pharmacological activities such as anti-imflammatory, anti-cancer, and anti-obesity activities that contribute to the therapeutic effects of the herb (Ho, Peh, Chan, & Wong, 2014; Kim, Seo, Liu, & Kim, 2014; Ko et al., 2016). Many bioactive chemical constituents from *A. annua* including artemisinin, flavonoids, terpenoids and their volatile oils have been well investigated (van der Kooy & Sullivan, 2013), but the high-molecular components such as polysaccharides have rarely been reported. Initial investigations indicated that *A. annua* polysaccharides can effectively inhibit hepatoma cell growth by improving the human body's cellular immune function and facilitating cell apoptosis (Chen, Wang, & Liu, 2014). However, the underlying molecular mechanism is still not elucidated. Therefore, in the present study, we first carried out experiments to isolate and characterize a purified polysaccharide from this plant, and then the underlying apoptotic mechanism of this polysaccharide was investigated in human hepatoblastoma G2 (HepG2) cell line. The results will be helpful for developing novel anti-tumor drugs.

2. Materials and methods

2.1. Materials and chemicals

The dried ground part of *Artemisia annua* L. (Hua Huahao) was purchased from a local grocery store in Chongqing (China). The Annexin V‐fluorescein isothiocyanate (FITC)‐propidium iodide (PI) Apoptosis kit was purchased from NanJing KeyGen Biotech Co., Ltd. (Nanjing, China). MTT (3-(4, 5-dimethyl-2-yl)-2, 5-diphenyl tetrazolium bromide), DAPI (2-(4-amidinophenyl)-6-indolecarbamidine dihydrochloride), T-series dextran (T-2000, T-70, T-40, T-20, and T-10) and monosaccharide standards (arabinose, rhamnose, galactose, glucose, mannose, fucose, xylose, glucoturonic acid and galacturonic acid) were obtained from Sigma Chemical Co. (St. Louis, MO). DEAE Sepharose fast flow and Sepharose CL-6B were purchased from Pharmacia Co. (Sweden). Antibodies for β-actin, Bcl-2, Bax, cytochrome c and NF-kappa B (kB)-p65 were purchased from Santa Cruz Biotechnology, Inc. (Santa Cruz, CA, U.S.A.). Horseradish peroxidase conjugated secondary antibodies and the enhanced chemiluminescence (ECL) detection system was purchased from Tiangen Biotech Co. (Beijing, China). Caspase-3, -8 and -9 activity assay kits were purchased from R&D Systems, Inc. (Minneapolis, MN, USA). Tissue culture media (RPMI 1640 and Eagle's Minimum Essential Medium) and fetal bovine serum (FBS) were from obtained GIBCO (Life Technologies, NY). Other reagents ($NaBH_4$, acetic anhydride, NaCl, phenol, sulphuric acid, chloroform, butanol, ethanol, $NaNO_3$, and 0.2% NaN_3) were obtained in the highest purity grade available commercially.

2.2. Isolation and purification of polysaccharide from A. annua

The dried *A. annua* L. (500 g) were powdered and defatted with 95% ethanol

(6000 mL) for three times and 2h each time. The residue (452g, 90.4% of dried raw material) was then air-dried at room temperature and extracted with boiling water (8000 mL) for 2 h and repeated for a total of three times. The extracts (20,230 mL) were filtered, combined, concentrated by evaporation and centrifuged at 1700 × *g* for 10 min at 4 °C. The resulting supernatant (5680 mL, 28.08% of the original total extract) was then concentrated and precipitated with 95% ethanol (4500 mL) for 24h at 4 °C. Following centrifugation (1700 × *g*, 10 min) at 4 °C, the obtained precipitation (20.5g, 4.1% of dried raw material) was re-dissolved in water in 400 mL and added with 100 mL of Sevag reagent (chloroform:butanol 4:1, v/v) to remove free protein in the samples for five times (Sevag, Lackman, & Smolens, 1938). The combined supernatant (255 mL) was further concentrated and dialyzed at –40 °C under 25 Psi pressure against running water for three days. The retentate was concentrated, centrifuged, and lyophilized under the same conditions to give crude *A. annua* polysaccharides (CAAP, 7.7g).

CAAP (7.7 g) was dissolved in 20 mL deionized water, centrifuged, and the supernatant was loaded on a DEAE Sepharose fast flow column (2.0 cm × 40cm, Cl^- form), eluted with deionized water and a gradient of 0–1.0 M NaCl solution at a flow rate of 2 mL/min to give three fractions (CAAP1, CAAP2 and CAAP3). All tubes (5 mL/each) were quantified by phenol-sulphuric acid method. The deionized water-eluted fraction CAAP1 (4.12g) was collected and dissolved in 20 mL deionized water, and centrifuged again to prepare the supernatant. Then each aliquot of this supernatant (5ml) was further purified by gel chromatography on a Sepharose CL-6B

column (2.5 × 80 cm) eluted with deionized water at a flow rate of 0.3 mL/min to yield a white power fraction, designated as AAP. This operation was repeated for four times to yield of total 3.25g of AAP.

2.3. Physicochemical and structural analysis of polysaccharide

2.3.1. Chemical component analysis

Total carbohydrate content of the polysaccharide was measured according to the phenol–sulfuric acid method (Dubois et al., 1956). Protein content of the polysaccharide was quantified by the method of Bradford (1976). Uronic acid content of the polysaccharide was detected by *m*-hydroxydiphenyl colorimetric method (Blumenkrantz & Asboe-Hansen, 1973).

2.3.2. Monosaccharide composition analysis

A unit of 10 mg samples was hydrolyzed with 2 M TFA (2 ml) at 120° C for 2 h in a sealed test tube. After removing TFA with methanol, the mixture of neutral monosaccharides was reduced with $NaBH_4$ and acetylated with acetic anhydride (York, Darvill, McNeil, Stevenson, & Albersheim, 1985). After those procedures, the acetylated products were re-dissolved in chloroform and performed on Shimadzu 2014 GC instrument (Shimadzu Co., Kyoto, Japan) equipped with a flame ionization detector (FID) and a HP-1 capillary column (30 m × 0.25 mm × 0.25 μm). The GC temperature was programmed at 120 °C for 3 min, followed by a 3◦C/min gradient up to 220 °C and held at 220 °C for 3 min. N_2 was used as the carrier gas and myo-inositol was used as an internal standard at a constant flow rate of 1 mL/min.

2.3.3. Homogeneity and molecular weight determination

The homogeneity and averaged molecular weight was determined by HPGPC instrument with an SHIMADZU HPLC system equipped with a TSK-G3000PWXL column (7.8 mm ×300 mm) and a SHIMADZU RID-10A refractive index detector. The mobile phase was composed of 0.1 mol/L $NaNO_3$ and 0.2% NaN_3, and the flow rate through the HPLC column was 0.7 ml/min at 40 °C with 1.6 mpa. The samples were dissolved in mobile phase as 0.3% (w/v) solution, centrifuged and 20 µl of the supernatant was injected in each run. The averaged molecular weight was estimated from the calibration curve of the elution volume of Dextran standards (T 130, 80, 50, 20, 10).

2.3.4. Ultraviolet (UV) spectroscopy analysis

The contents of protein and nucleic acid were determined using a Shimadzu UV-2401 spectrometer (Shimadzu, Japan) and scanned in the range of 190-500 nm (Makarova, Patova, Shakhmatov, Kuznetsov, & Ovodov, 2013).

2.3.5. IR spectroscopy analysis

Fourier-transform infrared (FTIR) spectrum of the polysaccharide was recorded with a Nicolet Nexus 470 spectrometer (Thermo Nicolet Co., Madison, WI, USA) by KBr method. Briefly, the polysaccharide dried at 35–44 °C in vacuum over P_2O_5 for 48 h was mixed with KBr powder, ground and then pressed into a 1-mm pellet for FTIR spectral measurements in the frequency range of 400–4000 cm^{-1} (Zhao, Dong, Chen, & Hua, 2010).

2.3.6. Methylation analysis

The vacuum-dried polysaccharide were methylated three times as described by Needs and Selvendran (1993) with a minor modification. Complete methylation was confirmed by the disappearance of the hydroxyl peak in the IR spectrum. The resulting permethylated product was depolymerized with 90% HCOOH at 100 °C for 3 h followed by hydrolysis with 2 M TFA at 100 °C for another 4 h. completely methylated polysaccharide was hydrolyzed with 2 ml of 2 M TFA, then, then reduced and acetylated as described by Sweet, Shapiro, and Albersheim (1975). A gas chromatograph–mass spectrometer (GC-MS) was used to analyse the glycosidic linkage on the basis of relative retention time and fragmentation pattern, and the molar ratios were calibrated using the peak areas and response factors of the FID in GC.

2.3.7. Nuclear magnetic resonance (NMR) analysis

The polysaccharide samples were kept with P_2O_5 in vacuum for one week before exhaustively being exchanged with 99.96% D_2O using intermediate freeze drying method. The deuterium-exchanged polysaccharides (60 mg) were dissolved in 0.6 ml of 99.96% D_2O in which 30µl acetone-d6 was added and then placed in 5 mm NMR tubes. Then, the ^{1}H, ^{13}C and 2D NMR (HMBC) spectra of AAP were performed by Bruker spectrometer (Bruker Corp., Zurich, Switzerland) at 400 MHz at 30 °C.

2.4. Cell lines and culture conditions

Human hepatoblastoma HepG2, human ovarian cancer cells SKOV3, breast

cancer cells MCF-7 and lung adenocarcinoma cells A549 were obtained from the Committee on Type Culture Collection of Chinese Academy of Sciences (Shanghai, China). SKOV3 and A549 cells were maintained in RPMI 1640 supplemented with 10% heat-inactivated FBS, 100 IU penicillin/ml and 100 µg streptomycin/ml. MCF-7 and HepG2 cancer cells were maintained in Eagle's minimum essential medium with 10% FBS, 100 IU penicillin/ml and 100 µg streptomycin/ml. All cultured cells were incubated at 37 °C in a humidified atmosphere containing 5% CO_2 in the air.

2.5. Cell proliferation assay

Cell viability was measured quantitatively by using MTT, showed the activity of living cells (Plumb, Milroy, & Kaye, 1989). Briefly, cancer cells were cultured to 80% confluence in 96-well culture plates (1×10^5 cells/well) and then treated with indicated concentrations of AAP (0, 5, 10, 20, 40, 80, and 160 µg/mL) for different indicated period. 50 µl of 5 mM MTT solution was then added to each well and the cell was cultured in dark for another 4 h. Thereafter, culture fluid was removed and 100 µL dimethyl sulfoxide (DMSO) was added to each well to dissolve purple formazan crystals, and then the absorbance was read at 540 nm on a 96-well plate reader. The absorbance of untreated cells was considered as 100%. The results were determined by three independent experiments.

2.6. DAPI staining assay

Morphological observation of nuclear change was assayed with a DNA-binding fluorescent dye DAPI to determine whether AAP induces apoptosis or not. After

treatment with or without AAP (40 μg/mL) for 24 h, the cells were washed three times with ice-cold PBS, fixed in a 4% formaldehyde solution for 20 min at 4 °C, then stained with 5 μg/ml DAPI for 1 h in the dark prior to visualization of blue fluorescence under a fluorescence microscope (OLYMPUS, Essex, U.K.).

2.7. Cell apoptosis assay by flow cytometry

The extent of apoptosis was determined using Annexin V‐FITC‐PI Apoptosis kit as described by the manufacture's instruction. Briefly, after exposure to AAP (10, 20, and 40 μg/mL) for 24 hours, cells were harvested, washed twice with PBS and followed by gentle centrifugation. The resulting cell pellet was resuspended in binding buffer (2.5 μl Annexin V-FITC, 5 μl PI). Non- AAP treated cells were collected as the control. After being incubated in the dark for 15 min, samples were assessed by a FACScan flow cytometer (Coulter EPICS XL, Beckman Coulter Inc., CA) and 10,000 cells were evaluated in each sample. Annexin V-positive and PI-positive cells were recognized as necrotic cells, while Annexin V-positive but PI-negative cells were regarded as apoptotic cells. The percentage of cells undergoing apoptosis was determined by three independent experiments

2.8. Analysis of caspase activities

Activity of caspase--3, -8 or -9 was quantified using a colorimetric assay kits according to the manufacturer's protocol. Briefly, cancer cells treated with AAP (10, 20, and 40 μg/mL) for 24 h or untreated control cells were lysed in 50 ml of cold lysis buffer and then cell lysates were collected and centrifuged at 12, 000 × g for 10 min at

4 °C. The resulting supernatants were collected to evaluate caspase activity. For each reaction, 10 μg total proteins were added to 50μl reaction buffer, followed by the additional 5μL of substrates specific for caspase-3, -8, or -9, respectively, and transferred into a 96-well plate for 4 h incubation at 37 °C in a CO_2 incubator. Finally, absorbance was measured at 405 nm. Caspase activities were expressed relative to theoretical density value (OD).

2.9. Preparation of cytosolic and mitochondrial fractionations and Western blotting analysis

For isolation of total protein fractions, treated or untreated cells were collected, washed twice with ice-cold PBS, and resuspended in cell lysis buffer and then incubated on ice for 15 min. The cell lysates were harvested by centrifugation at 12,000 g for 20 min at 4 °C to yield the supernatants for Western blot analysis. To examine the cytochrome c release from mitochondria, the cytosolic and mitochondrial extracts were prepared using mitochondrial fraction kit as per the manufacturer's instruction. Protein concentrations of the samples were quantified by the method of Bradford (1976).

Western blotting analyses were performed as described by Xin et al. [9] In brief, each equivalent amount of total proteins (30 μg) were electrophoresed on 10–12% SDS-PAGE gel and transferred onto nitrocellulose membranes, and then blocked with 5% (w/v) non-fat dry milk and incubated with specific primary antibodies (anti-β-actin, anti-Bcl-2, anti-Bax, anti-cytochrome c and anti-NF-kB) at a 1:1000

dilution in blocking solution. After thrice washings in TBST for each 5min, membranes were incubated with horseradish peroxidase conjugated secondary antibodies at a dilution of 1:500 in blocking solution for 1 h at room temperature. Finally protein bands were visualized with the aid of an enhanced chemiluminescence system (ECL) system.

2.10. RT-PCR

Total RNA was extracted from AAP-treated cells with a Trizol RNA isolation kit (Invitrogen Inc, CA, USA) and stored at −80 °C for subsequent analysis. First-stranded cDNA was synthesized with 5 μg total RNA by RT-PCR kit according to the manufacturer's instruction. The sequences of primers used in RT-PCR were as follows: Bax, 5'-TCCACCAAGAAGCTGAGCGA-3' (forward) and 5'-GTCCAGCCCATGATGGTTCT-3' (Reverse); Bcl-2, 5'-CTACGAGTGGGATGCGGGAGATG-3' (forward) and 5'-GGTTCAGGTACTCAGTCATCCACAG3' (Reverse); NF-kB, 5'-ATCCCAGGTTTCTTGCCTCT-3' (forward) and 5'-GGAGCACAGATACCACCAAGA-3' (Reverse); β-actin, 5'-TCACCCTGAAGTACCCCATC-3' (forward) and 5'-CCATCTCTTGCTGCAAGTCC-3' (Reverse). All of the primers used in RT-PCR were used to produce the correlated products, respectively. Amplification condition: one denaturing cycle at 94 °C (5min), 30 cycles at 94 °C (45 s), at appropriate Tm (1 min), at 72 °C (45 s), and a final extension at 72 °C (7 min). Finally, PCR products were run on 1.5 percent agarose gel electrophoresis and DNA bands were visualized

by ethidium bromide staining. All experiments were performed in triplicate.

2.11. Statistical analysis

The results were expressed as mean ± SD (standard deviation). Statistical differences were evaluated using the two-tailed Student's t-test and values of $p < 0.05$ were considered significantly different.

3. Results and discussion

3.1. Isolation, purification and general chemical properties of the polysaccharide

Crude polysaccharides, CAAP, were obtained with a yield of 1.54% (w/w) from *A. annua* through ethanol degreasing, hot-water extraction followed by ethanol precipitation, deproteinization by Sevag method, dialysis with water and lyophilization. CAAP was separated and fractionated on a DEAE Sepharose fast flow column stepwise with distilled water and a NaCl gradient (0–1.0 M) to give three elution peaks (titled as CAAP1, CAAP2 and CAAP3) (**Fig. 1A**). CAAP1 was further purified by a Sepharose CL-6B column eluted with deionized water to yield on purified fraction (**Fig. 1B**), named as AAP, with a yield of 0.65% (w/w). AAP contained 93.8% of carbohydrates as determined by phenol–sulfuric acid assay. Determination of protein and uronic acid suggested that AAP was free of proteins and was a neutral polysaccharide. The HPGPC profile of AAP exhibited a single and symmetrically sharp peak, which revealing it is a homogeneous polysaccharide (**Fig. 1C**). Based on the calibration with standard dextrans, its average molecular weight

was estimated to be about 6.3×10^4 Da. Moreover, GC analysis revealed that AAP consisted of glucose (Glc) and rhamnose (Rha) in the molar ratios of 4: 1 (**Fig. 2**), which indicated that the AAP was heterogeneous.

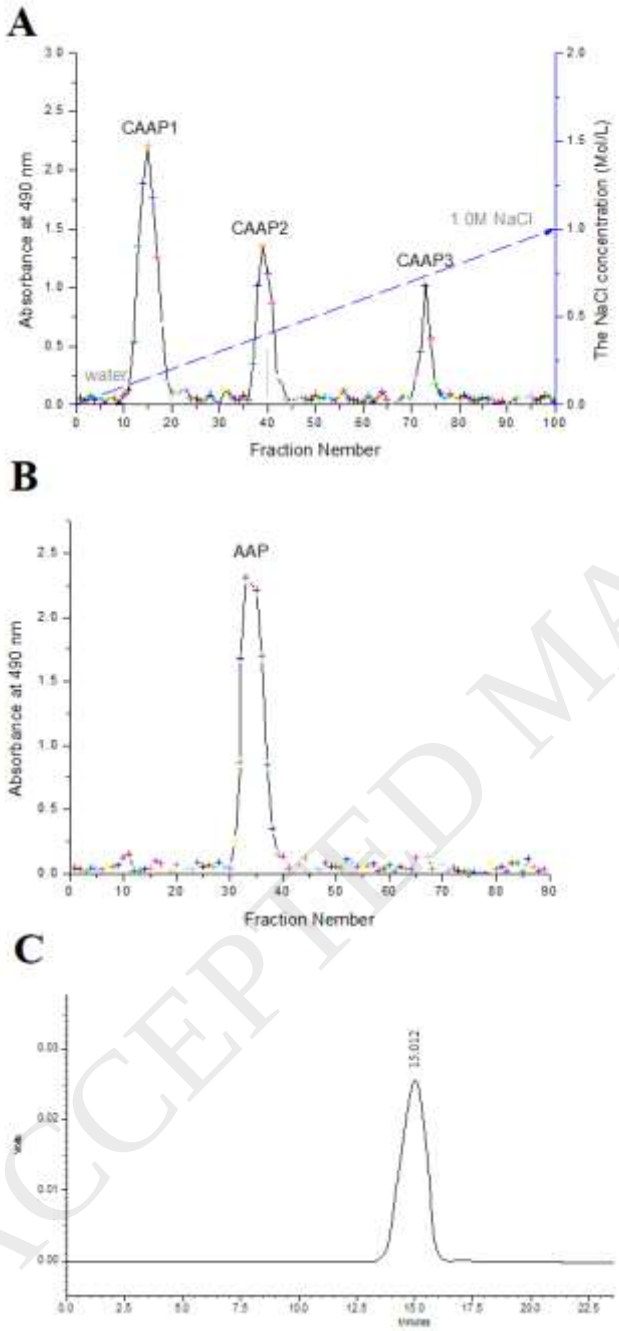

Fig. 1. (A) Isolation and purification of CAAP on a DEAE Sepharose fast flow column; (B) Isolation and purification of CAAP1 on a Sepharose CL-6B gel

filtration column. (C) HPGPC chromatogram of AAP

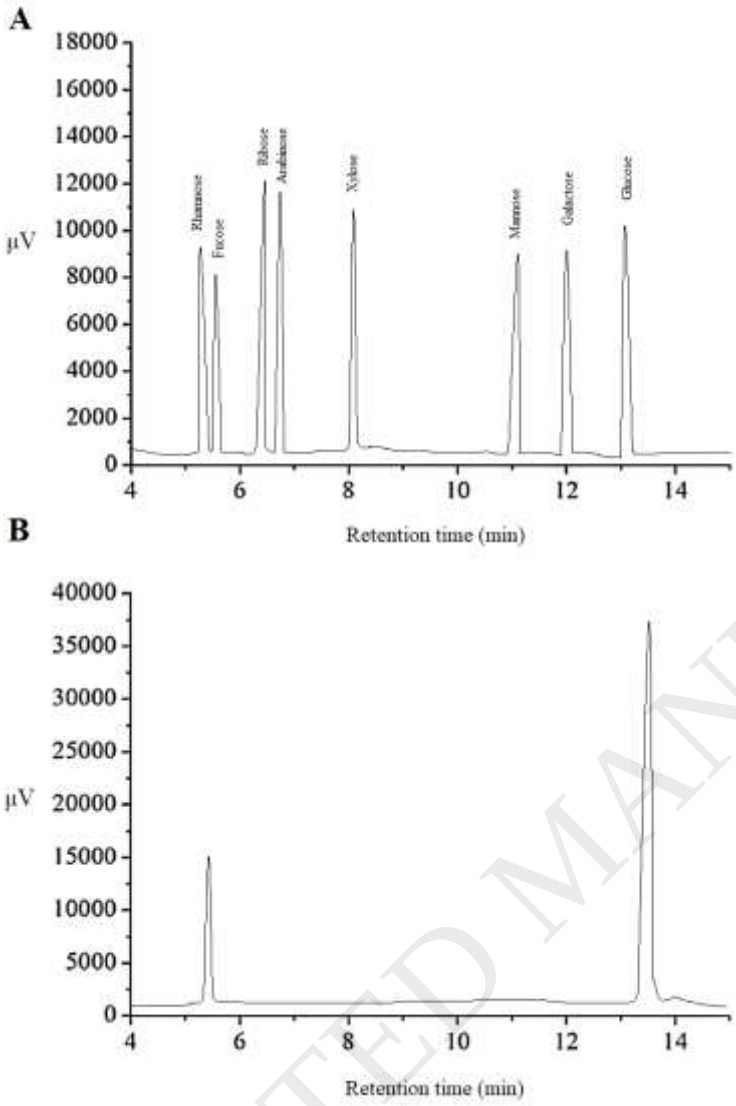

Fig. 2. (A) Gas chromatograms of the mixed standard monosaccharides. (B) Gas chromatograms of AAP

3.2. UV and IR spectrum analysis

A negative response to the Bradford test and no significant absorption peak in the UV spectrum between wavelengths from 190 to 500 nm illustrated the absence of protein and nucleic acid (**Fig. 3A**). FT-IR spectrum of AAP shown in **Fig. 3B** exhibited the typical absorption of polysaccharides. The characteristic strong broad

band at 3408.52 cm^{-1} and the weak bands 2936.67 cm^{-1} were the stretch vibrations of O-H and C-H, respectively (Zha et al., 2014). The absorption band at 1370.61 cm^{-1} was assigned to C-H bending vibration and the band at 1636.82 cm^{-1} was due to the presence of bound water. The peaks in the range of 1036.21–1146.85 cm^{-1} were attributed to the stretching vibration of C-O-C group. The freedom of band around 1720 and 1250 cm^{-1} indicated the absence of uronic acids and ester sulfate in the sample, which supported the results of uronic acids assay and UV analysis. Moreover, a characteristic absorption at 616.70 cm^{-1} was also observed, indicating the α-configuration of the sugar units.

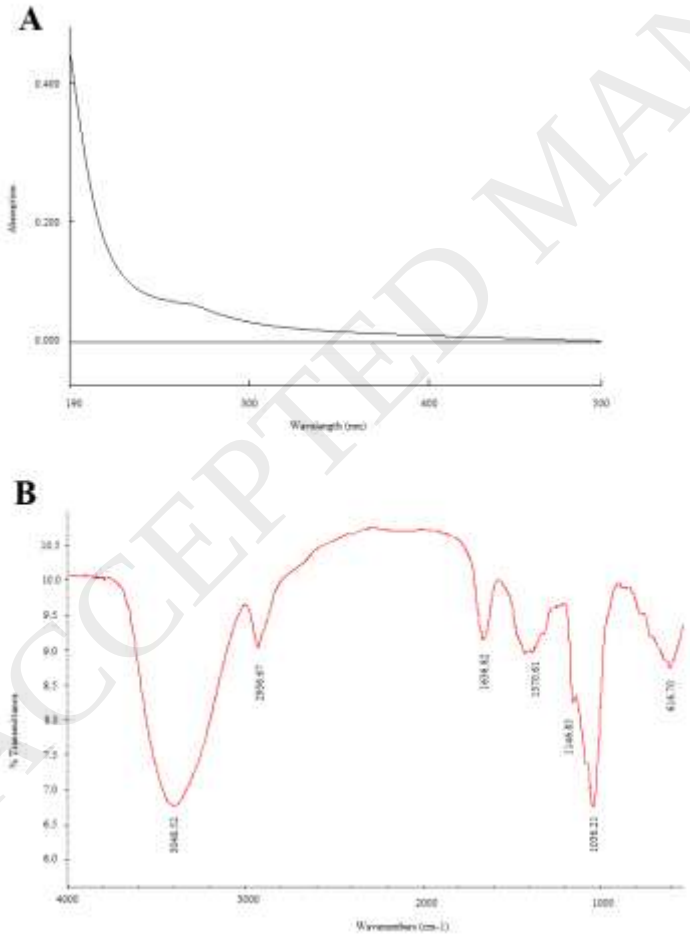

Fig. 3. (A) UV spectrum of AAP. (AB) FT-IR spectrum of AAP

3.3. Glycosyl linkages analysis

To determine the linkages of the monosaccharides in AAP, the fully methylated product of AAP was depolymerized, hydrolyzed, acetylated, and analyzed by GC–MS analysis. The individual peaks of methylated sugars from the GC-MS analysis were identified according to their retention times and by comparison with the mass spectrum. The GC–MS results indicated that the backbone chains were mainly 1, 4-linked Glcp (Residue-A, 2,3,6-Me_3-Glc) and 1, 3, 6-linked Glcp (Residue-B, 2,4-Me_2-Glc). The side chain attached to the O-6 position of Residue-B contained 1, 6-linked-Glcp (Residue-C, 2,3,4-Me_3-Glc), which was ended with single non-reducing terminal α-L-Rhap residue (Residue-D, 2,3,4-Me_3-Rha). According to the peak areas, four types of residues were seen in the ratio of 1: 1: 1: 1. The molar ratio of each monosaccharide was also in accordance with the results of GC.

The structural characteristics of AAP were further confirmed with ^{1}H and ^{13}C NMR spectral analysis. The proton signals between δ 3.0–5.5 and the carbon signals locating in the range of δ 60–110 are the characteristic signals of polysaccharide in NMR spectroscopy (Hu, Liang, & Wu, 2015). All ^{1}H NMR and ^{13}C NMR signals were summarized in **Table 1** based on the data available in literature (Liu, Sun, Yu, & Liu, L. 2012; Liu, Sun, Liu, & Yu, 2012; Maity et al., 2017; Molaei & Jahanbin, 2018; Ow, Green, Hao, & Mak, 2008; Shakhmatov, Belyy, & Makarova, 2018; Shakhmatov, Toukach, Kuznetsov, & Makarova, 2014) and depicted in **Fig. 4A** and **B,** respectively. It was clear from this figure that signals related to anomeric carbon were located in the range δ 97–101 ppm for 13C NMR and the peaks of anomeric protons fell in the

range of δ 5.0-5.2 ppm for ^{1}H NMR spectra, indicated that the presence of α-glycosidic configuration in AAP (Huang, Li, Li, & Wang, 2011). This result was in agreement with the glycosidic linkage types determined by IR. The signals at δ 99.56, 97.45, 99.96 and 101.35 ppm in ^{13}C NMR spectrum were attributed to the anomeric carbon atoms of Residue-A, Residue-B, Residue-C and Residue-D. The peaks at δ 78.45, 75.9, 69.8, and 68.75 ppm were coming from C4 of Residue-A, C3 of Residue-B, C6 of Residue-B and C6 of Residue-C, respectively. Similarly, the anomeric proton signals at δ5.10, 5.06, 5.03, and 5.15 in the ^{1}H NMR revealed the existence of Residue-A, Residue-B, Residue-C, and Residue-D. The strong signal at δ 4.70 ppm presented in the spectrum was attributed to HDO. In addition, a signal detected at δ 1.25 ppm in ^{1}H NMR and approximately δ 19.01 ppm in ^{13}C NMR which can be ascribed to H-6/C-6 methyl group of Rhap (Leone, Molinaro, Dubery, Lanzetta, & Parrilli, 2007).

The sequences of different sugar residues and the substitution sites were analyzed by observing the cross-peaks of both anomeric protons and carbons of glycosyl residues in HMBC spectrum after the assignments of 1H and 13C chemical shifts of all sugar residues. From the HMBC spectrum (**Fig. 4C**), we can observed correlations between the following anomeric protons and carbons at the linkage positions: C-4 (78.45) of residue A and H-1 (δ 5.03) of residue C (A C-4/C H-1), C-1 (99.96) of residue C and H-4 (δ 3.62) of residue A (C C-1/A H-4), C-3 (75.90) of residue B and H-1 (δ 5.10) of residue A (B C-3/A H-1), C-1 (99.56) of residue A and H-3 (δ 3.78) of residue B (A C-1/B H-3), C-6 (68.75) of residue C and H-1 (δ 5.06) of

residue B (C C-6/B H-1), C-1 (97.45) of residue B and H-6 (δ 3.87) of residue C (B C-1/C H-6). All these cross peaks suggested that there was a repeating structure fragment [→6)-α-D-Glcp-(1→4)-α-D-Glcp-(1→3,6)-α-D-Glcp-(1→) probably connected alternately in AAP as the linear backbone. Meanwhile the cross peaks at (δ 69.8/ 5.15) and e (δ 101.35/3.64) showed the correlation between C-6 of residue B and H-1 of residue D, and the correlation between C-1 of residue D and H-6 of residue B, respectively, indicating that the residue D was attached to C-6 of the residue B.

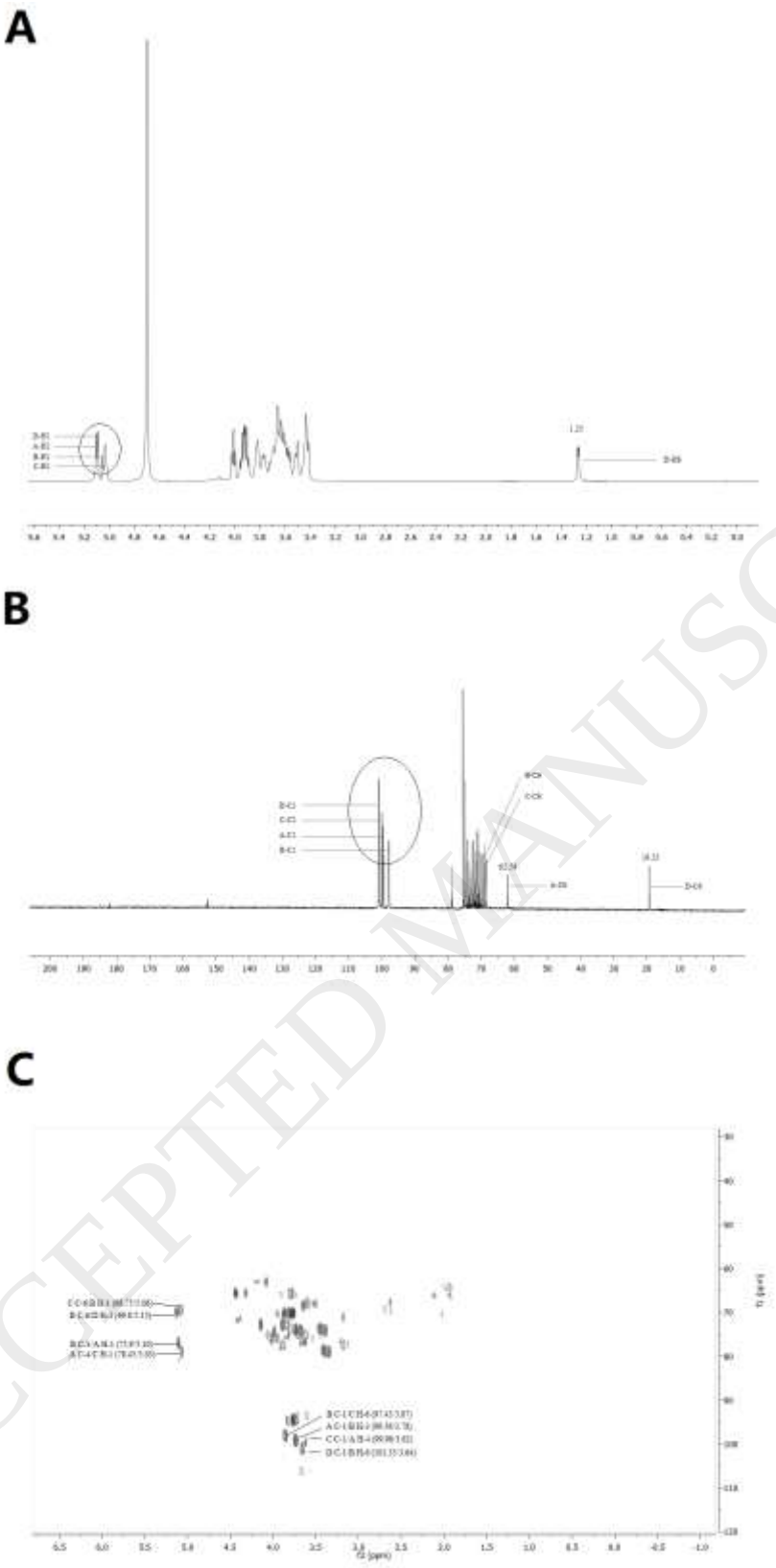

Fig. 4. (A) ^{1}H NMR spectrum of AAP. (B) ^{13}C NMR spectrum of AAP. (C) HMBC spectrum of AAP.

Table 1 Results of methylation analysis and ^{1}H and ^{13}C NMR chemical shifts of AAP

Methylated sugar	Linkage type	Molar ratios	MS fraction	Chemical shifts, δ (ppm)					
				C1/(H1)	C2/(H2)	C3/(H3)	C4/(H4)	C5/(H5)	C6/(H6)
2,3,6-Me_3-Glcp	Residue A →4)-α-D-Glcp-(1→	1	43,87,101,113, 117,129,131,233	99.56/5.10	72.12/3.50	72.78/3.74	78.45/3.62	71.06/3.87	62.54/3.62
2,4-Me_2-Glcp	Residue B →3,6)-α-D-Glcp-(1→	1	57,87,99,117,129,1 59,173,233	97.45/5.06	72.7/3.45	75.9/3.78	72.7/3.61	72.0/3.76	69.8/3.64
2,3, 4-Me_3-Glcp	Residue C →6)-α-D-Glcp-(1→	1	43,71,87,101,117,1 29,161,173, 189,233	99.96/5.03	72.31/3.89	74.62/3.76	71.04/3.59	69.99/3.85	68.75/3.87
2,3,4-Me_3-Rhap	Residue D α-L-Rhap-(1→	1	43,87,101,129,143, 189,203	101.35/5.15	72.08/4.06	72.92/3.60	73.32/3.67	69.87/4.03	19.01/1.25

On the basis of monosaccharide composition, methylation analysis and 1D and 2D NMR spectroscopy, the main structure of AAP was tentatively proposed in **Fig. 5** as follows:

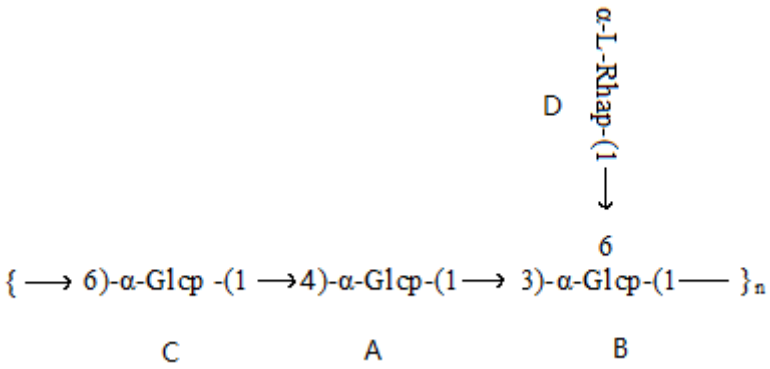

Fig. 5. Structure of AAP

3.4. AAP reduced viability of various cancer cells in vitro

To investigate the potential cytotoxicity of AAP, the comparative cytotoxic effects of AAP on cell viability were evaluated in four different cell lines: HepG2, SKOV3, MCF-7 and A549 cells by MTT assay (**Fig. 6A**). Exposure to AAP for 24 hours resulted in a decrease in cell viability in a dose-dependent manner in all cell lines, with an IC50 range of 20.87-69.05 μg/ml. The average IC50 for HepG2, SKOV3, MCF-7 and A549 were approximately 20.87, 43.25, 69.05, 58.54 μg/ml, respectively. Clearly, human ovarian cancer HepG2 cell line was the most susceptible cell line to AAP treatment. Thus further investigations were performed using HepG2 cells to evaluate antitumor activity of AAP (10, 20 and 40μg/ml) and to identify its underlying molecular mechanism.

3.5. AAP induced the apoptosis of HepG2 cells

To assess whether the growth inhibitory effects of AAP on HepG2 cells was associated with apoptosis, both control and AAP-treated cells were stained with the fluorescent DAPI nuclear dye and visualized by a fluorescent microscope. As shown in **Fig. 6B**, typical characteristics of apoptotic morphologic alterations, such as nuclear chromatin condensation, nuclear fragmentation, and formation of apoptotic bodies, were apparent in cells after exposure to AAP (40 μg/ml) for 24 h; in contrast, no evidence of abnormal nuclear morphology was present in the control group, which displayed intact and healthy nuclei. It suggested that AAP might induce ovarian cancer cell apoptosis.

To further quantify the apoptosis caused by AAP on HepG2 cells, the percentages of apoptotic cells were analyzed using flow cytometry (**Fig. 7A**). After 24 hours treatment with different concentrations of AAP, the numbers of early and late apoptotic cells were significantly dose-dependently increased as compared to control group ($P<0.05$ or $P<<0.01$). The percentage of total apoptotic cells in control cells was 0.64%, 36.85% in cells treated with 10 μg/ml of AAP, 48.24% in cells treated with 10 μg/ml of AAP and 64.78% in cells treated with 40 μg/ml of AAP (**Fig. 7B**). All these results demonstrated that HepG2 cells undergo apoptosis in response to AAP treatment.

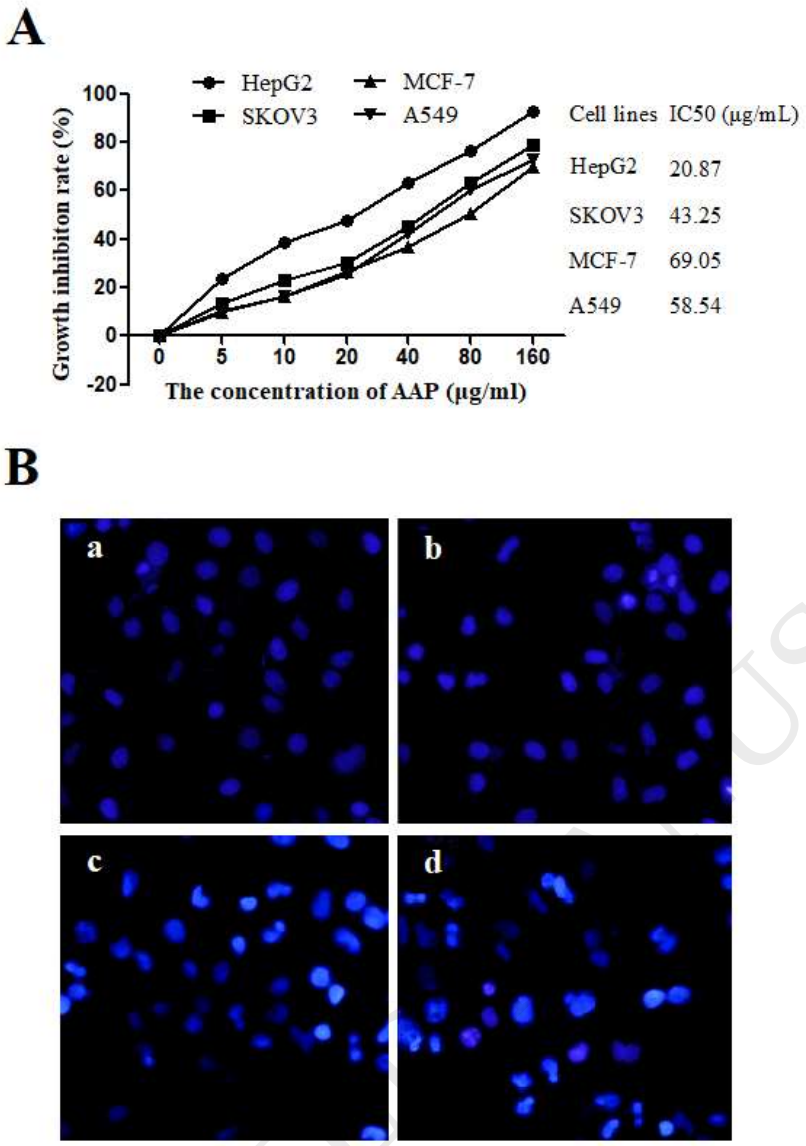

Fig. 6. (A) Effect of AAP on the proliferation of various human cancer cells. (B) Nuclear morphological changes induced by AAP in HepG2 cells after DAPI staining (×100). (a) Control (untreated) cells; (b) cells treated with 10μg/ml AAP; (c) cells treated with 20μg/ml AAP; (d) cells treated with 40μg/ml AAP. The experiments were repeated three times.

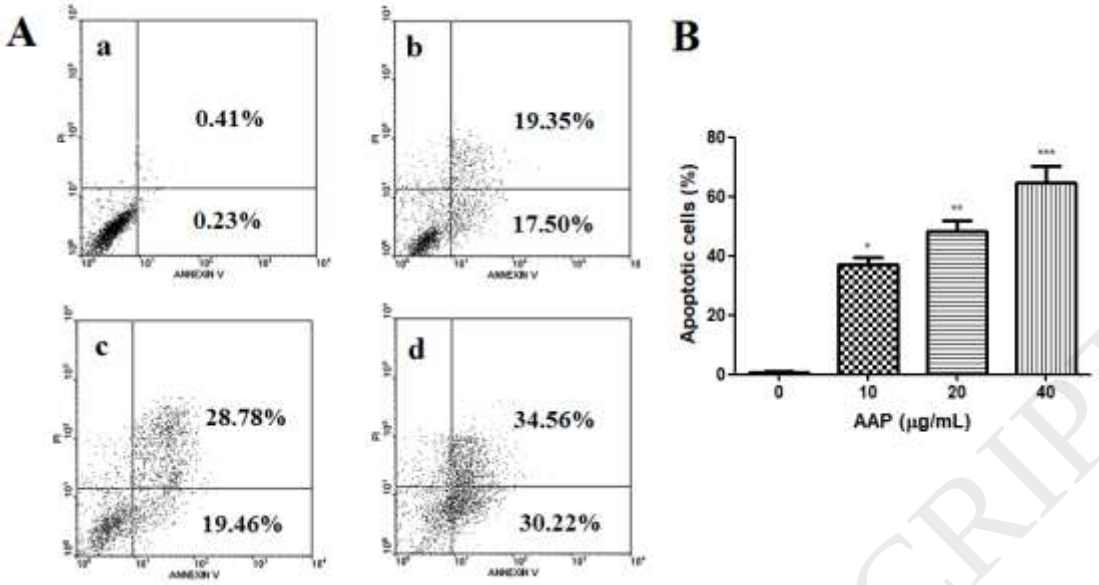

Fig. 7. (A) Flow cytometric analysis of AAP induced apoptosis in HepG2 cells using annexinV-FITC and PI double staining. (a) Control (untreated) cells; (b) cells treated with 10μg/ml AAP; (c) cells treated with 20μg/ml AAP; (d) cells treated with 40μg/ml AAP. (B) Quantitative presentation of apoptosis induced by AAP in HepG2 cells. The experiments were repeated three times. * $P < 0.05$, ** $P < 0.01$ compared to the control group

3.6. AAP activated caspase-3, -8 and -9

A molecular hallmark of apoptosis is the activation of caspases, which are a family of intracellular aspartate-specific cysteine proteases that execute cell death through proteolytic cleavage in the induction of apoptosis (Stennicke & Salvesen, 1998). Once initiator caspases are activated, such as caspase 8 or caspase 9, which would activate other downstream caspase-3 in response to pro-apoptotic signals, thus lead to the execution stage of apoptosis (Philchenkov, 2004; Salvesen & Dixit, 1999). Different initiator caspases are usually associated with specific pathways. For

example, caspase 9 is involved in the intrinsic (mitochondrial-dependent) apoptotic pathway and caspase 8 is typically linked with the initiation of the extrinsic (death receptor-dependent) pathway (Cho & Choi, 2002; Gogvadze, Orrenius, & Zhivotovsky, 2006; Scaffidi et al., 1998). However, there is increasing evidence for interaction and crosstalk between these two pathways (Chen & Wang, 2002; Michael, 2000). To examine whether caspase activation contributes to AAP-induced apoptosis, the activities of initiator caspase (caspase-8 and-9) and effector caspase (caspase- 3) were assessed by colorimetric assay kits after treatment of HepG2 cells with AAP (10, 20 and 40 μg/ml) for 24 h. The results showed a concentration-dependent increase in the activities of caspase-8, -9, and -3 in AAP-treated cells (**Fig. 8A**). Treatment of HepG2 cells with AAP at 10, 20 and 40μg/ml for 24 h increased 1.4-fold, 1.6-fold and 1.7-fold of the caspase-8 activity, and 1.9-fold, 2.2-fold and 2.4 fold of the caspase-9 activity, respectively. A similar change of caspase 3 activity was also observed and increased 2.3-fold, 2.7-fold and 2.9-fold when the cells were exposed to 10, 20 and 40μg/ml of AAP after 24 h treatment. These data suggest the simultaneous involvement of both the extrinsic and intrinsic apoptotic pathways in AAP-induced apoptosis in HepG2 cells; however this apoptotic mechanism is more dependent on intrinsic pathway as illustrated by a much more pronounced increase of caspase-9 activity and less activation of caspase 8.

3.7. AAP attenuated Bcl-2/Bax ratio and NF-kB expression, as well as mitochondrial release of cytochrome c

The event of the release of cytochrome c from mitochondria into the cytosol

plays an important role in mitochondria-dependent apoptotic pathway (Gogvadze, Orrenius, & Zhivotovsky, 2006). Once cytosol cytochrome c binds to apoptotic protease activating factor 1 (Apaf-1), the formation of Apaf-1/cytochrome c complexes allows the recruitment of caspase-9, then the latter trigger caspase-3 activation, thus resulting in execution of cell death (Green & Reed, 1998). What's more, Bid, a proapoptotic member of the Bcl-2 family, was induced to the cleaved form by caspase-8 also trigger cytochrome c release (Green, 1998). To confirm whether AAP induced apoptosis through a mitochondria-dependent pathway, proteins in both mitochondrial and cytosolic fractions were prepared and analyzed with western blot. Treatment of HeLa cells with 10, 20 and 40 μg/ml of AAP caused concentration dependent release of cytochrome c from mitochondria to cytosol, as evidenced by a gradual decrease in mitochondrial cytochrome c and a concomitant increase in the cytosolic fraction (**Fig. 8B**). These results indicate that AAP can promote cytochrome c release from mitochondria into cytosol.

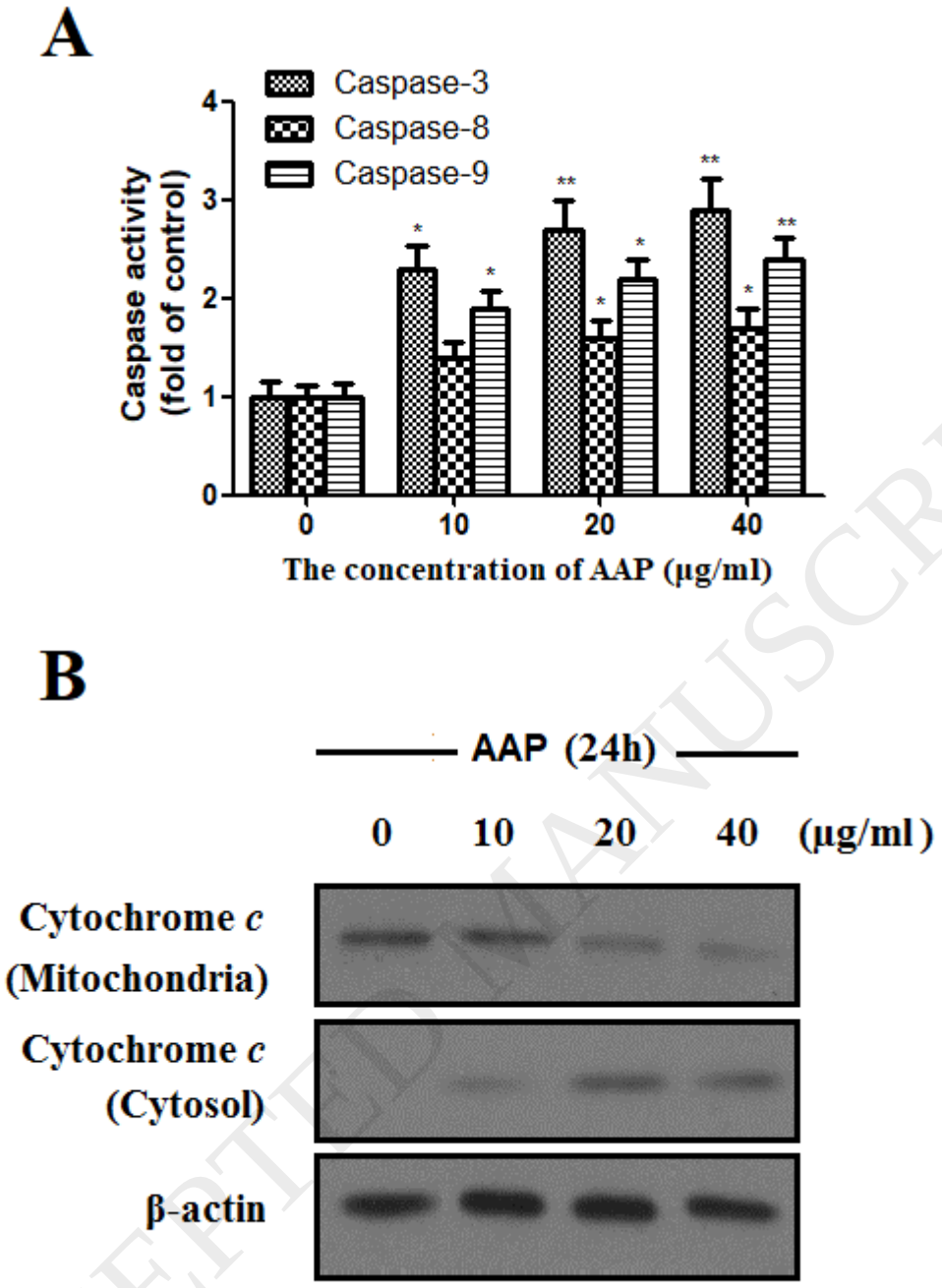

Fig. 8. (A) Effect of AAP on caspase-3, -8 and -9 activities in HepG2 cells. (B) Effect of AAP on the protein expression of cytochrome c in HepG2 cells. The experiments were repeated three times. * $P < 0.05$, ** $P < 0.01$ compared to the control group.

It is well known that the release of cytochrome c from mitochondria to cytosol is

controlled by multiple stimuli, the most prominent one being members of Bcl-2 family, which was composed of mainly two kinds of apoptosis regulators, namely pro-apoptotic (e.g. Bax) as well as anti-apoptotic (e.g. Bcl-2) members (Kirkin, Joos, & Zörnig, 2004). Importantly, the alteration in the balance between Bcl-2 and Bax has been recognized as critical regulators in controlling the release of mitochondrial cytochrome c to decide cell's susceptibility to apoptosis. Bax provoke the release of cytochrome c, whereas Bcl-2 blocks cytochrome c efflux by binding to the outer mitochondrial membrane (Ow, Green, Hao, & Mak, 2008). Thus, decreased Bax/Bcl-2 ratio promotes the release of cytochrome c from mitochondria into cytosol that in turn activates caspase-3 cleavage (Van Delft & Huang, 2006). There are an increasing amount of anti-cancer agents being capable of triggering the release of cytochrome c through either up-regulation of Bax and/or down-regulation of Bcl-2 (Li et al., 2014; Miao et al., 2013; Zou et al., 2015). To gain more insight into the mechanisms of AAP, we next analyzed the effect of AAP on the expression of Bax and Bcl-2 in HepG2 cells using RT-PCR and Western blot analysis. After exposure of HepG2 cells to AAP for 24h, Bax expression significantly increased, while Bcl-2 expression remains constant as determined by Western blot analysis (**Fig. 9A**). Up-regulation of Bax mRNA expression and unchanged of Bcl-2 mRNA expression in AAP-treated HepG2 cells were also confirmed by RT-PCR (**Fig. 9B**). Thus, balance between Bax and Bcl-2 was upset after AAP treatment in favor of a rise of Bax/Bcl-2 ratio, suggesting the involvement of Bcl-2 family proteins in AAP-induced apoptosis in HepG2 cells. These findings support the idea that AAP-induced apoptosis of HepG2 cells is at least

in part mediated via a mitochondrion-dependent apoptotic pathway.

It is well acknowledged that the activation of the extrinsic and intrinsic apoptotic pathways is highly influenced by multiple molecules such as Bcl-2 proteins, the PI3K pathway members, and the nuclear factor-κB (NF-κB) transcription factor family (Johnstone, Ruefli, & Lowe, 2002; Viktorsson, Lewensohn, & Zhivotovsky, 2005). In ovarian tumors, activation of NF-κB pathway promotes aggressive tumor phenotypes, including cell survival, migration, invasion, angiogenesis, stem cell-like properties, and resistance to therapy (Sethi, Sung, & Aggarwal, 2008). Therefore, inhibition of the proteasomal degradation of NF-κB has been used as a rationale for development of anti-ovarian cancer therapies. Because NF-κB subunits, particularly p65, are a major regulator of cell survival and apoptosis (Dutta, Fan, Gupta, Fan, & Gelinas, 2006; Karin & Lin, 2002), we examined the protein and mRNA expression of NF-κB p65 in HepG2 cells following AAP treatment. Both Western blot and RT-PCR analysis identified that AAP abrogates the expression of NF-κB p65 in a dose-dependent manner in HepG2 cancer cells, suggesting the involvement of NF-κB p65 in AAP-mediated mitochondrion-dependent apoptotic pathway (**Fig. 9C and D**).

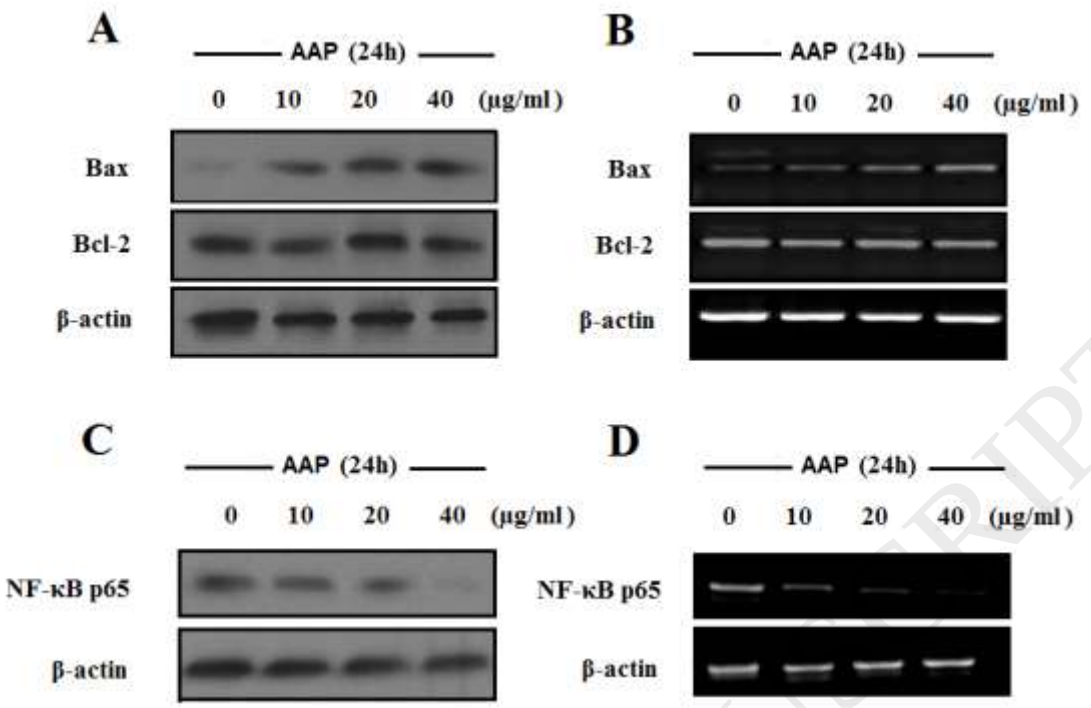

Fig. 9. (A) Effect of AAP on the protein expression of Bax and Bcl-2 in HepG2 cells. (B) Effect of AAP on the mRNA expression of Bax and Bcl-2 in HepG2cells. (C) Effect of AAP on the protein expression of NF-κB p65 in HepG2 cells. (D) Effect of AAP on the mRNA expression of NF-κB p65 in HepG2 cells.

4. Conclusions

In conclusion, the present study showed the data for the first time that AAP inhibited the growth of HepG2 cells in a dose-dependent manner, and this reduction in cell viability predominantly resulted from the p65-dependent mitochondrial signaling pathway, as evidenced by strong activation of caspase-3 and -9, the release of cytochrome c from mitochondria into cytosol, and increased ratio of pro-apoptotic and anti-apoptotic Bcl-2 family proteins (Bax/Bcl-2). In addition, piperine-induced

apoptosis is also closely associated with decreasing expression of NF-κB p65 in HepG2 cells, which subsequently triggers apoptotic pathways, resulting in apoptosis. These findings provides insight into molecular mechanism for the anticancer activity of AAP toward human ovarian cancer cells and suggests that AAP may be a candidate for further evaluation as a cancer preventive and chemotherapeutic agent, especially for human ovarian cancer. Further studies on the in vivo activity of AAP towards HepG2 xenograft tumors in nude mice are in progress.

References

Bagchi, D., Bagchi, M., Stohs, S. J., Das, D. K., Ray, S. D., Kuszynski, C. A., et al. (2000). Free radicals and grape seed proanthocyanidin extract: importance in humanhealth and disease prevention. *Toxicology, 148(2),* 187–197.

Blumenkrantz, N., & Asboe-Hansen, G. (1973). New method for quantitative determination of uronic acids. Analytical Biochemistry, 54, 484–489.

Bradford, M. M. (1976). A rapid and sensitive method for the quantitation ofmicrogram quantities of protein utilizing the principle of protein-dye binding. *Analysis Biochemistry, 72,* 248–254.

Chen, J., Wang, X., & Liu, C. (2014). Anti-tumour effects of polysaccharides isolated from Artemisia Annua L by inducing cell apoptosis and immunomodulatory

anti-hepatoma effects of polysaccharides. *African Journal of Traditional, Complementary and Alternative Medicines, 11(1),* 15–22.

Chen, J., Yao, D., Yuan, H., Zhang, S., Tian, J., Guo, W., et al. (2013). Dipsacus asperoides polysaccharide induces apoptosis in osteosarcoma cells by modulating the PI3K/Akt pathway. *Carbohydrate polymers, 95(2),* 780–784.

Chen, M., & Wang, J. (2002). Initiator caspases in apoptosis signaling pathways. *Apoptosis, 7(4),* 313-319.

Cho, S. G., & Choi, E. J. (2002). Apoptotic signaling pathways: caspases and stress-activated protein kinases. *BMB Reports, 35(1),* 24-27.

Dubois, M., Gilles, K. A., Hamilton, J. K., Rebers, P. A., & Smith, F. (1956).Colorimetric method for determination of sugars and related substances. *Analysis Chemistry, 28,* 350–356.

Dutta, J., Fan, Y., Gupta, N., Fan, G., & Gelinas, C. (2006). Current insights into the regulation of programmed cell death by NF-κB. *Oncogene, 25(51),* 6800-6816.

Gogvadze, V., Orrenius, S., & Zhivotovsky, B. (2006). Multiple pathways of cytochrome c release from mitochondria in apoptosis. *Biochimica et Biophysica Acta (BBA)-Bioenergetics, 1757(5),* 639-647.

Green, D. R. (1998). Apoptotic pathways: the roads to ruin. *Cell, 94,* 695–698.

Green, D. R., & Reed, J. C. (1998). Mitochondria and apoptosis. *Science, 281,* 1309–1312.

Ho, W. E., Peh, H. Y., Chan, T. K., & Wong, W. F. (2014). Artemisinins: pharmacological actions beyond anti-malarial. *Pharmacology & Therapeutics, 142(1),* 126–139.

Hu, H., Liang, H., & Wu, Y. (2015). Isolation, purification and structural characterization of polysaccharide from Acanthopanax brachypus. *Carbohydrate Polymers, 127,* 94-100.

Huang, S. Q., Li, J. W., Li, Y. Q., & Wang, Z. (2011). Purification and structural characterization of a new water-soluble neutral polysaccharide GLP-F1-1 from Ganoderma lucidum. *International Journal of Biological Macromolecules, 48,* 165-169.

Johnstone, R. W., Ruefli, A. A., & Lowe, S. W. (2002). Apoptosis: a link between cancer genetics and chemotherapy. *Cell, 108(2),* 153-164.

Karin, M., & Lin, A. (2002). NF-κB at the crossroads of life and death. *Nature Immunology, 3(3),* 221-227.

Kim, M. H., Seo, J. Y., Liu, K. H., & Kim, J. S. (2014). Protective effect of Artemisia annua L. extract against galactose-induced oxidative stress in mice. *PloS one, 9(7),* e101486.

Kirkin, V., Joos, S., & Zörnig, M. (2004). The role of Bcl-2 family members in tumorigenesis. *Biochimica et Biophysica Acta (BBA)-Molecular Cell Research, 1644(2),* 229-249.

Ko, Y. S., Lee, W. S., Panchanathan, R., Joo, Y. N., Choi, Y. H., Kim, G. S., et al. (2016). Polyphenols from Artemisia annua L Inhibit Adhesion and EMT of Highly Metastatic Breast Cancer Cells MDA-MB-231. *Phytotherapy Research, 30(7),* 1180–1188.

Krishna, R., & Mayer, L. D. (2000). Multidrug resistance (MDR) in cancer: mech-anisms, reversal using modulators of MDR and the role of MDR modulatorsin influencing the pharmacokinetics of anticancer drugs. *European Journal of Pharmaceutical Sciences, 11(4),* 265–283.

Leone, S., Molinaro, A., Dubery, I., Lanzetta, R., & Parrilli, M. (2007).The O-specific polysaccharide structure from the lipopolysaccharide of theGram-negative bacterium Raoultella terrigena. *Carbohydrate Research, 342,*1514–1518

Li, C., Tian, Z. N., Cai, J. P., Chen, K. X., Zhang, B., Feng, M. Y., Shi, Q. T., Li, R., Qin, Y., & Geng, J. S. (2014). Panax ginseng polysaccharide induces apoptosis by targeting Twist/AKR1C2/NF-1 pathway in human gastric cancer. *Carbohydrate Polymers, 102,* 103-109.

Li, C., Wu, X., Zhang, H., Yang, G., Hao, M., Sheng, S., et al. (2015). A Huaier polysaccharide reduced metastasis of human hepatocellular carcinoma SMMC-7721 cells via modulating AUF-1 signaling pathway. *Tumor Biology, 36(8),* 6285–6293.

Liu, G., Sheng, Y., Zhang, M., & Sun, D. (2016). A polysaccharide from the leaves of Aralia elata induces apoptosis in U-2 OS cells via mitochondrial-dependent

pathway. *International Journal of Biological Macromolecules, 93,* 418-425.

Liu, J., Sun, Y., Yu, C., & Liu, L. (2012). Chemical structure of one low molecular weight and water-soluble polysaccharide (EFP-W1) from the roots of Euphorbia fischeriana. *Carbohydrate Ppolymers, 87,* 1236-1240.

Liu, J., Sun, Y., Liu, L., & Yu, C. (2012). A water-soluble polysaccharide (EFP-AW1) from the alkaline extract of the roots of a traditional Chinese medicine, Euphorbia fischeriana: Fraction and characterization. *Carbohydrate Ppolymers, 88,* 1299-1303.

Maity, P., Nandi, A. K., Manna, D. K., Pattanayak, M., Sen, I. K., Bhanja, S. K., et al. (2017). Structural characterization and antioxidant activity of a glucan from Meripilus giganteus. Carbohydrate polymers, 157, 1237-1245.

Makarova, E. N., Patova, O. A., Shakhmatov, E. G., Kuznetsov, S. P., & Ovodov, Y. S. (2013). Structural studies of the pectic polysaccharide from Siberian fir (Abiessibirica Ledeb.). *Carbohydrate Polymers, 92,* 1817–1826.

Miao, S., Mao, X., Pei, R., Miao, S., Xiang, C., Lv, Y., Yang, X., Sun, J., Jia, S., & Liu, Y. (2013). Lepista sordida polysaccharide induces apoptosis of Hep-2 cancer cells via mitochondrial pathway. *International Journal of Biological Macromolecules, 61,* 97-101.

Michael, O. (2000). The biochemistry of apoptosis. *Nature, 407,* 770–776.

Molaei, H., & Jahanbin, K. (2018). Structural features of a new water-soluble

polysaccharide from the gum exudates of Amygdalus scoparia Spach (Zedo gum). *Carbohydrate Polymers, 182*, 98-105.

Needs, P. W., & Selvendran, R. R. (1993). Avoiding oxidative degradation during sodium hydroxide/methyl iodide-mediated carbohydrate methylation in dimethyl sulfoxide. *Carbohydrate Research, 245*, 1–10.

Ow, Y. L. P., Green, D. R., Hao, Z., & Mak, T. W. (2008). Cytochrome c: functions beyond respiration. *Nature Reviews Molecular Cell Biology, 9(7)*, 532-542.

Pei, J. J., Wang, Z. B., Ma, H. L., & Yan, J. K. (2015). Structural features and antitumor activity of a novel polysaccharide from alkaline extract of Phellinus linteus mycelia. *Carbohydrate Polymers*, *115*, 472-477.

Philchenkov, A. (2004). Caspases: potential targets for regulating cell death. *Journal of Cellular and Molecular Medicine, 8(4)*, 432-444.

Plumb, J. A., Milroy, R., & Kaye, S. B. (1989). Effects of the pH dependence of 3-(4, 5-dimethylthiazol-2-yl)-2, 5-diphenyltetrazolium bromide-formazan absorption on chemosensitivity determined by a novel tetrazolium-based assay. *Cancer Research, 49(16),* 4435-4440.

Räth, K., Taxis, K., Walz, G., Gleiter, C. H., Li, S. M., & Heide, L. (2004). Pharmacokinetic study of artemisinin after oral intake of a traditional preparation of Artemisia annua L.(annual wormwood). *The American Journal of Tropical Medicine and Hygiene, 70(2),* 128–132.

Salvesen, G. S., & Dixit, V. M. (1999). Caspase activation: the induced-proximity model. *Proceedings of the National Academy of Sciences, 96(20),* 10964-10967.

Scaffidi, C., Fulda, S., Srinivasan, A., Friesen, C., Li, F., Tomaselli, K. J., Debatin, K. M., & Peter, M. E. (1998). Two CD95 (APO- 1/Fas) signaling pathways. The EMBO journal, 17(6), 1675-1687.

Sethi, G., Sung, B., & Aggarwal, B. B. (2008). Nuclear factor-κB activation: from bench to bedside. *Experimental Biology and Medicine, 233(1),* 21-31.

Sevag, M. G., Lackman, D. B., & Smolens, J. (1938). The isolation the components ofstreptococcal nucleoproteins in nucleoproteins in serologic ally active form. *Journal of Biological Chemistry, 124,* 425–436.

Shakhmatov, E. G., Belyy, V. A., & Makarova, E. N. (2018). Structure of acid-extractable polysaccharides of tree greenery of Picea abies. *Carbohydrate Polymers, 199,* 320-330.

Shakhmatov, E. G., Toukach, P. V., Kuznetsov, S. P., & Makarova, E. N. (2014). Structural characteristics of water-soluble polysaccharides from Heracleum sosnowskyi Manden. *Carbohydrate Polymers, 102,* 521-528.

Stennicke, H. R., & Salvesen, G. S. (1998). Properties of the caspases. *Biochimica et Biophysica Acta (BBA)-Protein Structure and Molecular Enzymology, 1387(1),* 17-31.

Sun, Z., Huang, K., Fu, X., Zhou, Z., Cui, Y., & Li, H. (2014). A chemically sulfated

polysaccharide derived from Ganoderma lucidum induces mitochondrial-mediated apoptosis in human osteosarcoma MG63 cells. *Tumor Biology, 35(10),* 9919–9926.

Sweet, D. P., Shapiro, R. H., & Albersheim, P. (1975). Quantitative analysis by various g.l.c response-factor theories for partially methylated and partially ethylated alditol acetates. *Carbohydrate Research, 40,* 217–225.

Van Delft, M. F., & Huang, D. C. (2006). How the Bcl-2 family of proteins interact to regulate apoptosis. *Cell Research, 16(2),* 203-213.

van der Kooy, F., & Sullivan, S. E. (2013). The complexity of medicinal plants: The traditional Artemisia annua formulation, current status and future perspectives. *Journal of Ethnopharmacology, 150(1),* 1–13.

Viktorsson, K., Lewensohn, R., & Zhivotovsky, B. (2005). Apoptotic pathways and therapy resistance in human malignancies. *Advances in Cancer Research, 94,* 143-196.

Wang, Y., Chen, J., Zhang, D., Zhang, Y., Wen, Y., Li, L., & Zheng, L. (2013). Tumoricidal effects of a selenium (Se)-polysaccharide from Ziyang green tea on human osteosarcoma U-2 OS cells. *Carbohydrate polymers, 98(1),* 1186–1190.

Yang, B., Xiao, B., & Sun, T. (2013). Antitumor and immunomodulatory activity of Astragalus membranaceus polysaccharides in H22 tumor-bearing mice. *International Journal of Biological Macromolecules, 62,* 287-290.

York, W. S., Darvill, A. G., McNeil, M., Stevenson, T. T., & Albersheim, P. (1985). Isola-tion and characterization of plant cell walls and cell-wall components. *Methods of Enzymology, 118,* 3–40.

Zha, S. H., Zhao, Q. S., Chen, J. J., Wang, L. W., Zhang, G. F., Zhang, H., et al. (2014).Extraction, purification and antioxidant activities of the polysaccharides frommaca (Lepidium meyenii). *Carbohydrate Polymers, 111*, 584–587.

Zhao, L. Y., Dong, Y. H., Chen, G. T., & Hua, Q. H. (2010). Extraction, purification, characterization and antitumor activity of polysaccharides from Ganodermalucidum. *Carbohydrate Polymers, 80,* 783–789.

Zou, Y., Qin, X., Xiong, H., Zhu, F., Chen, T., & Wu, H. (2015). Apoptosis of human non-small-cell lung cancer A549 cells triggered by evodiamine through MTDH-dependent signaling pathway. *Tumor Biology, 36(7),* 5187-5193.